Article

Electron Dynamics in Charge-Transfer-to-Solvent States of Aqueous Chloride Revealed by Cl 2p Resonant Auger-Electron Spectroscopy

Bernd Winter, Emad F. Aziz, Niklas Ottosson, Manfred Faubel, Nobuhiro Kosugi, and Ingolf V. Hertel

J. Am. Chem. Soc., **2008**, 130 (22), 7130-7138 • DOI: 10.1021/ja8009742 • Publication Date (Web): 08 May 2008

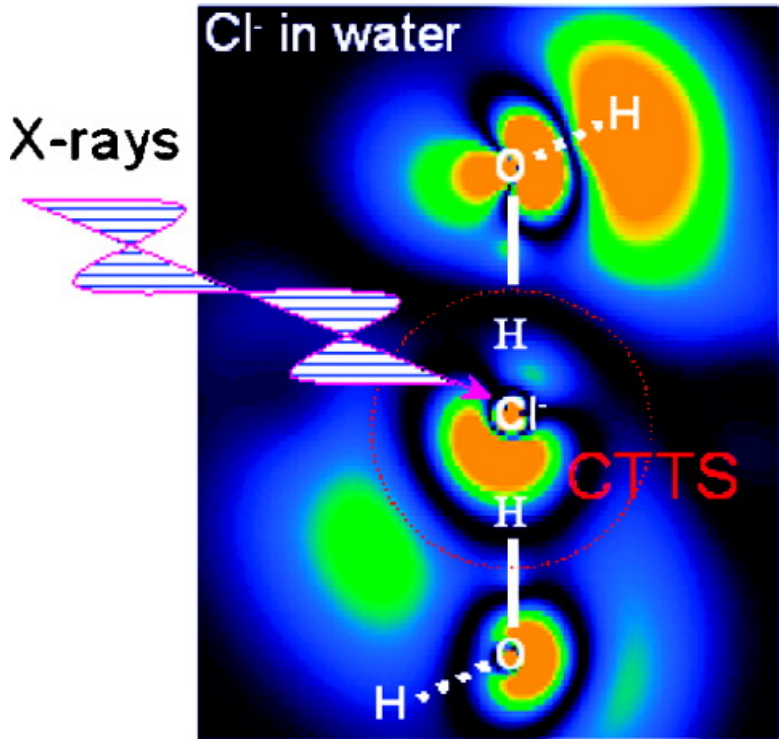

J|A|C|S
ARTICLES

Published on Web 05/08/2008

Electron Dynamics in Charge-Transfer-to-Solvent States of Aqueous Chloride Revealed by Cl^- 2p Resonant Auger-Electron Spectroscopy

Bernd Winter,*,† Emad F. Aziz,‡ Niklas Ottosson,‡,§ Manfred Faubel,|| Nobuhiro Kosugi,*,⊥ and Ingolf V. Hertel†,#

Max-Born-Institut für Nichtlineare Optik and Kurzzeitspektroskopie, Max-Born-Strasse 2A, D-12489 Berlin, Germany, BESSY, Albert-Einstein-Strasse 15, D-12489 Berlin, Germany, Department of Physics, Uppsala University, SE-75121 Uppsala, Sweden, Max-Planck-Institut für Dynamik and Selbstorganization, Bunsenstrasse 10, D-37073 Göttingen, Germany, UVSOR, Institute for Molecular Science, Myodaiji, Okazaki 444-8585, Japan, and Institut für Experimentalphysik, Freie Universität Berlin, Arnimallee 14, D-10195 Berlin, Germany

Received February 7, 2008; E-mail: bwinter@mbi-berlin.de; kosugi@ims.as.jp

Abstract: Charge-transfer-to-solvent (CTTS) excited states of aqueous chloride are studied by a novel experimental approach based on resonant inner-shell photoexcitation, Cl^-_{aq} 2p → e(*i*), $i = 1-4$, which denotes a series of excitations to lowest and higher CTTS states. These states are clearly identified through the occurrence of characteristic spectator Auger decays to double Cl 3p valence-hole states, where the CTTS states can be more stabilized as compared to single Cl^-_{aq} 2p core excitations and optical valence excitations. Furthermore, we have found for the first time that the CTTS electron e(*i*) bound by a single Cl 2p hole not only behaves as a spectator e(*i*) → e′(*i*), bound by a double valence-hole state before relaxation of the excited electron (*i*) itself, but also shows electron dynamics to the *relaxed* lowest state, e(*i*) → e′(1*). This interpretation is supported by ab initio calculations. The key to performing photoelectron and Auger-electron spectroscopy studies from aqueous solutions is the use of a liquid microjet in ultrahigh vacuum in conjunction with synchrotron radiation.

Introduction

Halide anions in aqueous solution exhibit intense absorption bands in the deep ultraviolet. These spectral features, which are strongly solvent-dependent, correspond to electron excitation into so-called charge-transfer-to-solvent (CTTS) states. Immediately after excitation the electron is bound in a potential well due to the pre-existing polarization of oriented solvent dipoles around the ion, and obviously no gas-phase analogue exists.[1] It is important to note that the CTTS electron is expected to be diffuse yet localized within the radius of the first solvation shell. CTTS states (or electron transfer spectra in the early literature) were first noticed approximately 75 years ago,[2] and comprehensive reviews with a first theoretical interpretation already appeared in 1942[3] and 1954.[4] An extensive, exhaustive account of optical CTTS transitions was given in 1970.[5] In the 1990s, a pioneering time-resolved study reported on the formation of the solvated electron in water via photoexcitation of the aqueous iodide CTTS.[6] Several subsequent pump−probe studies with subpicosecond laser pulses followed,[7–9] as well as theoretical quantum-state resolved simulations on the detachment dynamics of aqueous anions, including chloride.[10–13] More recently, with single-photon and multiphoton detachment, Bradforth and collaborators have systematically studied time-resolved scavenging and recombination dynamics, mostly for aqueous iodide CTTS.[1,14–18] In the case of the one-photon CTTS excitation the detachment process is thought to proceed through a rapidly collapsing metastable CTTS state,[12] a conclusion based

† Max-Born-Institut für Nichtlineare Optik and Kurzzeitspektroskopie.
‡ BESSY.
§ Uppsala University.
|| Max-Planck-Institut für Dynamik and Selbstorganization.
⊥ UVSOR, Institute for Molecular Science.
Freie Universität Berlin.

(1) Chen, X.; Bradforth, S. E *Annu. Rev. Phys. Chem.* **2008**, *59*, 203–231.
(2) Franck, J.; Haber, F. *Sitzungsberichte der Preussischen Akademie der Wissenschaften Physikalisch-Mathematische Klasse* **1931**, 250.
(3) Rabinowitch, E. *Rev. Mod. Phys.* **1942**, *14*, 0113.
(4) Platzmann, R.; Franck, J. *Z. Phys.* **1954**, *138*, 411.
(5) Blandamer, M. J.; Fox, M. F. *Chem. Rev.* **1970**, *70*, 59.
(6) Long, F. H.; Lu, H.; Shi, X. L.; Eisenthal, K. B. *Chem. Phys. Lett.* **1990**, *169*, 165.
(7) Gauduel, Y.; Gelabert, H.; Ashokkumar, M. *Chem. Phys.* **1995**, *197*, 167.
(8) Gelabert, H.; Gauduel, Y. *J. Phys. Chem.* **1996**, *100*, 13993.
(9) Assel, M.; Laenen, R.; Laubereau, A. *Chem. Phys. Lett.* **1998**, *289*, 267.
(10) Sheu, W. S.; Rossky, P. J. *Chem. Phys. Lett.* **1993**, *202*, 186.
(11) Staib, A.; Borgis, D. *J. Chem. Phys.* **1995**, *103*, 2642.
(12) Sheu, W. S.; Rossky, P. J. *J. Phys. Chem.* **1996**, *100*, 1295.
(13) Staib, A.; Borgis, D. *J. Chem. Phys.* **1996**, *104*, 9027.
(14) Kloepfer, J. A.; Vilchiz, V. H.; Lenchenkov, V. A.; Germaine, A. C.; Bradforth, S. E. *J. Chem. Phys.* **2000**, *113*, 6288.
(15) Kloepfer, J. A.; Vilchiz, V. H.; Lenchenkov, V. A.; Chen, X. Y.; Bradforth, S. E. *J. Chem. Phys.* **2002**, *117*, 766.
(16) Kloepfer, J. A.; Vilchiz, V. H.; Lenchenkov, V. A.; Bradforth, S. E. *ACS Symp. Ser., v820 2002* **2002**, *820*, 108.
(17) Vilchiz, V. H.; Chen, X. Y.; Kloepfer, J. A.; Bradforth, S. E. *Radiat. Phys. Chem.* **2005**, *72*, 159.
(18) Moskun, A. C.; Bradforth, S. E.; Thogersen, J.; Keiding, S. *J. Phys. Chem. A* **2006**, *110*, 10947.

 10.1021/ja8009742 CCC: $40.75

largely on measurements of the electron trapping time and ejection length,[14,19] and on nonadiabatic quantum dynamics as well as simulations to describe the electronic and solvent relaxation dynamics of photoexcited aqueous halides. This involves solvent rearrangement and short-range electron ejection into a caged pair $(I^o{:}e^-)_{aq}$. [1,12,14,15] The subject has recently been reviewed.[1]

Charge transfer in an aqueous environment plays a crucial role in numerous chemical and biological processes,[20] and threshold electron-ejection processes via photodetachment from a CTTS state provide very simple models for understanding solvent-controlled electron transfer reactions. Here, atomic CTTS solutes, having no intramolecular degrees of freedom, are particularly suited to monitor the local environment, specifically the motions of the solvent molecules driving electron transfer.[21] Moreover, due to the important role the solvent plays for the CTTS excited state, structural details of the solution such as ion-pair formation can be identified by the CTTS (optical) absorption spectra.[5] Also, the interaction of anions in electrolyte solutions with ionizing radiation is of considerable chemical-technical relevance.[20] An understanding of the underlying microscopic details remains, however, incomplete without the detailed characterization of the electronic structure of the solution. Hence, it is important to design experiments that identify solvent and solute species, in ground- and (transient) excited-electronic states, by their characteristic photoelectron or decay spectra. The present study tackles CTTS states by a novel experimental approach, using X-ray synchrotron radiation, in a range near 200 eV to excite CTTS states resonantly from a localized Cl 2p core in aqueous chloride (Cl^-_{aq}). Combined measurements of photoelectron and Auger-electron spectra from the aqueous chloride solution, when using photon energies near the Cl 2p edge, reveal several empty Cl^-_{aq} levels through the occurrence of so-called spectator Auger decays to double valence-hole states. Here, the CTTS states can be better stabilized, as supported by *ab initio* calculations. They are more definitely visible than those in single Cl 2p core excitations and in optical valence excitations. As the Auger process is extremely fast, i.e., on the order of the Cl 2p lifetime (approximately 6 fs[22]), the experiment probes CTTS electron dynamics almost at the instant the state is created. The experimental basis that makes the energy-resolved detection of (photo)electrons from highly volatile solvent/solvate systems possible is the recently developed liquid-microjet technique,[23–25] which produces a free liquid-water surface in a differentially pumped high-vacuum chamber.

Methods

Experimental. Photoemission (PE) studies of 3 molal (m) LiCl and 2 m NaCl aqueous solutions were performed at the soft X-ray undulator U41 PGM (180−1600 eV photon energy; approximately 10^{12} photons/s at a resolution of 4000) of the synchrotron radiation facility BESSY, Berlin. PE spectra were collected from a, typically, 15 μm diameter liquid microjet, having a velocity of approximately 80−100 m/s and a temperature of 4 °C. Under these conditions a flowing, free equilibrated liquid-water filament surface in vacuum is obtained,[23,24] and photoelectrons from the liquid phase can travel a sufficiently long distance (1−2 mm) without collisions with gas-phase water molecules. Also, at this small size and high streaming velocity of the jet, light-induced charging effects or radiolysis can be fully suppressed,[23] both of which usually severely complicate studies of liquids.[26] In the present experiment photoelectrons pass through $a \leq 200$-μm diameter orifice, which separates the main interaction chamber (operating at 10^{-5} mbar) from the differentially pumped detector chamber (operating at 10^{-9} mbar) housing a hemispherical electron energy analyzer, equipped with a multi-channel detector. The orifice is at a distance of <1.0 mm from the liquid jet. Electrons were detected normal to both the synchrotron light polarization vector and direction of propagation of the liquid jet, with an electron spectrometer acceptance angle of 12°. The energy resolution of the beamline was set to 0.2 eV, for 600 eV photon energy, and the resolution of the hemispherical energy analyzer was constant with kinetic energy (about 0.2 eV, at a pass energy of 20 eV). Typical photoelectron count rates were 10^3 s^{-1} at a photon energy of 600 eV. The small focal size of 23 × 12 μm^2 at this beamline assures a good matching spatial overlap between the synchrotron light beam and the liquid jet, which minimizes gas-phase contributions to the liquid spectrum. Further details of the experimental setup together with a discussion on the application of photoelectron spectroscopy to highly volatile aqueous solutions can be found in refs 24 and 25. Chemicals used for preparing the solutions were of the highest quality commercially available, and highly demineralized water was used for all experiments.

Ab Initio Calculations. The present theoretical method is an all-electron ab initio Hartree−Fock approach using Gaussian basis functions. We have used four different cluster models to simulate approximately 2 m NaCl and LiCl aqueous solutions, that is, 1 LiCl or NaCl and 29 H_2O or 31 H_2O in a volume of about $(10\ Å)^3$ (2 M aqueous solution ∼2 NaCl or LiCl and 56 H_2O). Ground-state geometries were optimized within the Hartree−Fock calculations using a 6-31G* basis set. We found several local minima from different initial guesses for the geometry, though we are not interested in the lowest state. We chose two local minima (models 1 and 2) for LiCl + 29·H_2O and a local minimum for NaCl + 29·H_2O and for NaCl + 31·H_2O. The initial guess of these geometries was chosen from a stable cluster of 30 H_2O molecules composed of five- and four-member water rings, where the center water molecule with five nearest neighbor water molecules was exchanged to either Cl or Na/Li. During geometry optimization, a NaCl + 29·H_2O cluster with Na^+ at the center showed that the Cl^- ion was coordinated by only four H_2O molecules on the surface of the cluster. Therefore, two additional H_2O molecules were added to find some local minima for NaCl + 31·H_2O. In these clusters, the distance between Cl and Na/Li is approximately 3.9−5.9 Å, and Cl^- is surrounded by five or six nearest-neighbor H_2O molecules. The long-range electrostatic interaction beyond a volume of approximately $(10\ Å)^3$ is partly improved by adding four sets of point charges (+1.0 and −1.0) at a distance of ∼10−15 Å from Cl^- to simulate LiCl or NaCl in the next cells, where the H_2O molecule itself is electrostatically weaker and is not taken into account.

The theoretical method for the Cl 2p ionized states (for describing photoionization) and Cl 3p doubly ionized states (for description of Auger decay) is also an all-electron ab initio Hartree−Fock approach taking into account Cl 2p and Cl 3p holes explicitly, using the GSCF3 code.[27,28] The spin−orbit interaction is neglected. The excited electrons e(*i*) corresponding to CTTS states are optimized

(19) Vilchiz, V. H.; Kloepfer, J. A.; Germaine, A. C.; Lenchenkov, V. A.; Bradforth, S. E. *J. Phys. Chem. A* **2001**, *105*, 1711.
(20) Garrett, B. C.; et al. *Chem. Rev.* **2005**, *105*, 355.
(21) Barthel, E. R.; Martini, I. B.; Schwartz, B. J. *J. Phys. Chem. B* **2001**, *105*, 12230.
(22) Fink, R. F.; Kivilompolo, M.; Aksela, H.; Aksela, S. *Phys. Rev. A* **1998**, *58*, 1988.
(23) Faubel, M.; Steiner, B.; Toennies, J. P. *J. Chem. Phys.* **1997**, *106*, 9013.
(24) Winter, B.; Faubel, M. *Chem. Rev.* **2006**, *106*, 1176.
(25) Winter, B.; Weber, R.; Widdra, W.; Dittmar, M.; Faubel, M.; Hertel, I. V. *J. Phys. Chem. A* **2004**, *108*, 2625.
(26) Lundholm, M.; Siegbahn, H.; Holberg, S.; Arbman, M. *J. Electron Spectrosc. Relat. Phenom.* **1986**, *40*, 163.
(27) Kosugi, N.; Kuroda, H. *Chem. Phys. Lett.* **1980**, *74*, 490.
(28) Kosugi, N. *Theor. Chim. Acta* **1987**, *72*, 149.

Table 1. Measured Auger-Electron Kinetic Energies (KE) of the Resonance Features at the Three Centerline Photon Excitation Energies E_1, E_2, and E_3, near the Cl^-_{aq} 2p Edge[a]

hv [eV]	KE [eV]	BE [eV]	TE [eV]	assignment
$E_1 = 201.0$	179.7	21.3	3.8	**2** [2hle′(2)]
	181.2	19.8	5.3	**1** [2hle′(1)]
$E_2 = 202.4$	177.0			**n** [2 h]
	178.5			**n** [2 h]
	179.9	22.5	2.6	**3** [2hle′(3)]
	182.3	20.1	5.0	**2** [2hle′(2*)]
	183.9	18.5	6.6	**1** [2hle′(1*)]
$E_3 = 204.0$	177.0			**n** [2 h]
	178.5			**n** [2 h]
	180.0	24.0	1.1	**4** [2hle′(4)]
	181.5	22.5	2.6	**3** [2hle′(3)]
	185.5	18.5	6.6	**1** [2hle′(1*)]

[a] Peak labels are the same as those used in Figures 2−4. The spectator Auger transitions from four spectator levels, 1h1e(*i*) to 2h1e′(*i*), are assigned using the binding energy (BE) and term energy (TE), because the spectator Auger final states show constant BE. TEs are evaluated by assuming DIP(Cl $3p^{-2}$) = 25.1 eV using BE($2p_{3/2}$) = 202.1 eV and BE($2p_{1/2}$) = 203.6 eV and the normal Auger KE($2p_{3/2}$) = 177.0 eV and KE($2p_{1/2}$) = 178.5 eV from Cl 2p single hole [1 h] to Cl 3p double hole [2 h]. 2h1e′(*i**) is a relaxed state and 2h1e′(*i*) is an unrelaxed state, where $i = 1$ or 2.

within the static exchange (STEX) method.[29,30] The ion cores in the STEX calculations are an average over the three Cl 2p core hole states with doublet spin coupling and the lowest Cl 3p double hole states with triplet spin coupling. The basis functions used are Cl (3112121/31121/1*), O (721/52), H (42), Na (421/31), and Li (31) taken from the contracted Gaussian-type functions Cl (533/53), O (73/7), H (6), Na (43/4), and Li (4) as proposed by Huzinaga et al.[31] The d-type polarization function used is $\zeta = 0.514$ for chlorine. The s-type diffuse functions are added on the Cl site to describe diffuse CTTS states around the Cl atom in aqueous solutions; the exponents are 0.0253, 0.01141, 0.00589, 0.00334, and 0.00204.[32] The results using the s, p, and d diffuse functions show main features (intensities) in the Cl 2p excitation that are not so different from the results using only s-type diffuse functions. In the present work the latter results are shown in Table 2 in order to simplify correlation between the CTTS states in the Cl 2p excitation and in the experimentally observed spectator Auger decay.

Results

Figure 1 shows the Cl^-_{aq} 2p photoemission (PE) spectrum from a 3 m LiCl aqueous solution measured at 400.2 eV photon energy. The horizontal upper axis in the figure displays electron binding energies (BE), and the bottom axis presents the measured electron kinetic energies (KE). From the peak maxima in the spectrum we find 202.1 and 203.6 eV vertical BE for Cl^-_{aq} $2p_{3/2}$ and Cl^-_{aq} $2p_{1/2}$, respectively, and the Cl^-_{aq} $2p_{3/2}$ photodetachment threshold energy, or appearance potential, is ∼200.5 eV. We can estimate the Cl^-_{aq} $2p_{1/2}$ photodetachment threshold at ∼202.0 eV. Considering the peak full width at half-maximum (fwhm) of 2.5 eV, the Cl^-_{aq} $2p_{3/2}$ ionization potential ranges from ∼200.5 eV to ∼203.5 eV, and for Cl^-_{aq} $2p_{1/2}$ they range from ∼202.0 eV to ∼205.0 eV. In aqueous solution the peak width arises from the heterogeneous, instantaneous distribution of solvation shell configurations, and the same width is measured at higher resolution. The 2p spin−orbit splitting of 1.5 eV observed here is by 0.5 eV smaller than that for gas-phase chlorine (Cl_2),[33] but it is almost identical with the splitting in solid NaCl or KCl.[34] This reduced spin−orbit interaction indicates that the 2p orbital in the Cl^- anion is more extended than that in the neutral Cl and can be correlated with the band-like electronic structure in aqueous solution. At a photon energy of 400.2 eV used for the spectrum of Figure 1 additional, broad emission lines are observed in the 160−190 eV KE range. The dominant one, with a maximum intensity at 177.6 eV KE, arises from Cl^-_{aq} *LMM*-Auger-electron emission (AE), where the *LMM*-Auger means that the final states have two additional holes (3s, 3p) in the *M* shell after filling the hole (2p) in the *L* shell, and it is observed here for the first time in an aqueous phase.

Photoelectron spectra of 3 m LiCl aqueous solution that were recorded for a series of photon energies from 198.8−204.8 eV, i.e., in the vicinity of the Cl^-_{aq} 2p BE, are presented in Figure 2. The spectra are displayed as a function of the measured KE, the photoelectron yield being normalized to the photon flux. The KEs correspond to ∼5−35 eV BE, covering electrons from the lowest binding-energy in solution (Cl^-_{aq} 3p with 9.6 eV BE [35]) at the high-KE end to the water $2a_1$ (30.9 eV BE[25]) electron at the low-KE end. Except for contributions that may arise from resonant excitations these are the valence PE spectra of the solution. The bottom spectrum of Figure 2 was measured at a photon energy of 198.8 eV, i.e., just slightly below the Cl^-_{aq} $2p_{3/2}$ photodetachment threshold and exclusively contains contributions from direct valence photoemission. No features from Auger decay appear at this photon energy. The peaks at 167.9, 181.5, 185.3, 187.6, and 189.2 eV KE (corresponding to 30.9, 17.3, 13.5, 11.2, and 9.6 eV BE) arise from photoelectron emission from the water orbitals $2a_1$, $1b_2$, $3a_1$, $1b_1$, and Cl^-_{aq} 3p, [24,25] respectively. The very small peak at 180 eV KE, corresponding to 19.2 eV BE, is due to electron detachment from a Cl^-_{aq} 3s orbital. Notice that the lowest-energy Li^+ orbital, Li^+_{aq} 1s, has a BE of 60.4 eV,[35] which is outside the range displayed in Figure 2.

When increasing the photon energy additional peaks are expected to appear in the valence PE spectra. The most obvious contribution is the Auger-electron peak at 177.6 eV KE (of Figure 1), which should be visible once the photon energy has exceeded the L-edge, i.e., the Cl^-_{aq} $2p_{3/2}$ and Cl^-_{aq} $2p_{1/2}$ detachment thresholds, 200.5 and 202.0 eV. These *off*-resonance normal Auger components, labeled **n** for $2p_{3/2}$ and **n** for $2p_{1/2}$ hole (intermediate) state, are indeed observed experimentally for photon energies larger than 202.0 eV. Although the Cl^-_{aq} $2p_{3/2}$ (Cl^-_{aq} $2p_{1/2}$) ionization potential ranges from 200.5 to 203.5 eV (202.0 to 205.0 eV), we assume here nonresonant Auger electrons are emitted with a constant KE, in principle independent of excitation energy,[36] that is, through a normal Auger process. Hence, the respective peaks do not shift with photon-energy in Figure 2, whereas the KEs of the direct PE electrons (constant BE) increase linearly. When raising the photon energy beyond 202 eV, **n** and **n** intensities gradually increase, and in addition further normal Auger peaks with approximately 10%

(29) Iwata, S.; Kosugi, N.; Nomura, O. *Jpn. J. Appl. Phys.* **1978**, *17*, 109.
(30) Kosugi, N.; Adachi, J.; Shigemasa, E.; Yagishita, A. *J. Chem. Phys.* **1992**, *97*, 8842.
(31) Huzinaga, S.; Andzelm, J.; Kolbukowski, M.; Radzio-Andzelm, E.; Sakai, Y.; Tatewaki, H. *Gaussian Basis Sets for Molecular Calculations*; Elsevier: Amsterdam, 1984.
(32) Kaufmann, K.; Nager, C.; Jungen, M. *Chem. Phys.* **1985**, *95*, 385.
(33) Lide, D. R. *Handbook of Chemistry and Physics*; CRC Press: Boca Raton, FL, 1997.
(34) Moulder, J. F.; Stickle, W. F.; Sobol, P. E.; Bomberg, K. D. *Handbook of X-ray Photoelectron Spectroscopy*; Perkin-Elmer Corporation: 1992.
(35) Winter, B.; Weber, R.; Hertel, I. V.; Faubel, M.; Jungwirth, P.; Brown, E. C.; Bradforth, S. E. *J. Am. Chem. Soc.* **2005**, *127*, 7203.
(36) Hüfner, S. *Photoelectron Spectroscopy: Principles and Applications*; Springer-Verlag: Berlin, Heidelberg, New York, London, Paris, Tokyo, Hong Kong, Barcelona, Budapest, 1995.

Table 2. Term Energies (TEs) (in parentheses, orbital size in Å) and Binding Energies (BEs) in eV of *s*-type CTTS Electrons in the Cl 2p Core-Ionized State and in the Lowest Cl (3p)^4 Triplet Final State after the Normal Auger Decay, Calculated Using Four Different Cluster Models of ~2 M NaCl and LiCl Aqueous Solutions[a]

	LiCl+29·H_2O model 1	LiCl+29·H_2O model 2	NaCl+29·H_2O	NaCl+31·H_2O	expmt for $2p_{3/2}$	expmt for $2p_{1/2}$
			$Cl^2[2p^{-1}]$			
BE	204.26	204.36	204.18	204.32	202.1	203.6
TE[1hle(1)]	2.47 (6.7)	2.62 (6.2)	2.56 (6.0)	2.77 (6.2)		2.6
TE[1hle(2)]	1.79 (8.7)	1.84 (9.6)	1.86 (8.9)	1.84 (9.7)	1.1	1.2
TE[1hle(3)]	0.95 (12.4)	0.95 (12.6)	0.97 (12.5)	0.98 (12.4)	−0.3	−0.4
TE[1hle(4)]	0.54 (18.0)	0.54 (18.0)	0.55 (18.0)	0.56 (18.0)	−1.9	
			$Cl^3[3p^{-2}]$			
DIP	26.63	26.88	26.51	27.04	25.1	
TE[2hle′(1*)]	6.84 (4.1)	7.09 (4.6)	7.09 (4.0)	7.23 (4.8)	6.6	
TE[2hle′(1)]	4.64 (6.7)	5.64 (6.2)	5.35 (6.0)	6.03 (6.2)	5.3	
TE[2hle′(2)]	3.33 (8.7)	2.98 (9.6)	3.28 (8.9)	2.82 (9.7)	3.8	
TE[2hle′(3)]	2.98 (12.4)	2.11 (12.6)	2.19 (12.5)	2.10 (12.4)	2.6	
TE[2hle′(4)]	1.10 (18.0)	1.38 (18.0)	1.14 (18.0)	1.13 (18.0)	1.1	

[a] 2h1e′(*i*) is calculated by assuming the same e(*i*) as in 1h1e(*i*). 2h1e′(1*) is a relaxed state and 2h1e′(1) is an unrelaxed state.

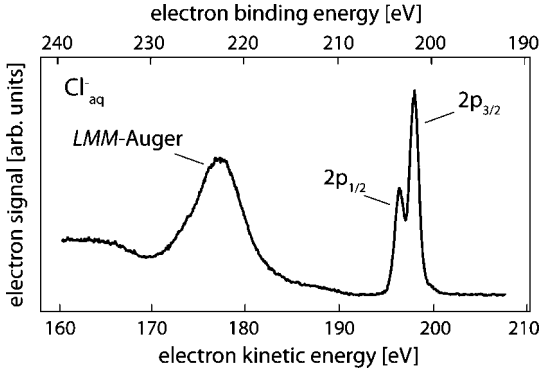

Figure 1. Cl^-_{aq} 2p photoelectron spectrum of 3 m LiCl aqueous solution measured at a photon energy of 400.2 eV. The top axis presents electron binding energies (BEs), and the bottom axis shows electron kinetic energies (KEs). The Cl^-_{aq} $2p_{3/2}$ and Cl^-_{aq} $2p_{1/2}$ BEs are 202.1 and 203.6 eV, respectively. The broad peak at 177.6 eV KE is due to chloride(aq) normal *LMM*-Auger emission.

intensity of the *LMM* main signal can be seen near 167 eV KE (Figure 2, trace c). These peaks arise from Cl^-_{aq} 3s to Cl^-_{aq} 2p core filling.

Much more remarkable, in addition to the off-resonance features, resonance spectral peaks appear for certain narrow ranged values of the photon energy *hν*, marked in the series of Figure 2 by numbers. They are associated with the promotion of a Cl^-_{aq} 2p electron into a given empty chloride(aq) state interacting with solvent−water molecules. The origin of these extra signals is a spectator Auger decay, giving rise to small peaks at 179.7 eV (peak **2**) and 181.2 eV KE (peak **1**). **2** and **1** exhibit maximum intensities at a photon energy $E_1 = 201.0$ eV (Figure 2, trace a), which is just below the Cl^-_{aq} $2p_{3/2}$ detachment threshold energy. Intensities drop to zero at photon energies near 200.4 and 201.8 eV, indicative of a resonance total width of about 1.4 eV and with a fwhm of ~0.7 eV, only. The underline of the labels indicates that the initial excitation is from the Cl $2p_{1/2}$ level (as opposed to Cl $2p_{3/2}$, which is not underlined). We realize that the detection of the small spectator peaks, on top of a strong water signal background, is quite fortunate in our experiment and can easily go undetected at poorer statistics of the experimental data. Furthermore, we should notice that the final states reached after the spectator Auger decay have the same electron configuration as the valence shakeup ionization (3p ionization with simultaneous single 3p → empty-state excitation into a two-hole one-electron 2h1e state), where the spectator electron (1e) is bound by two Cl

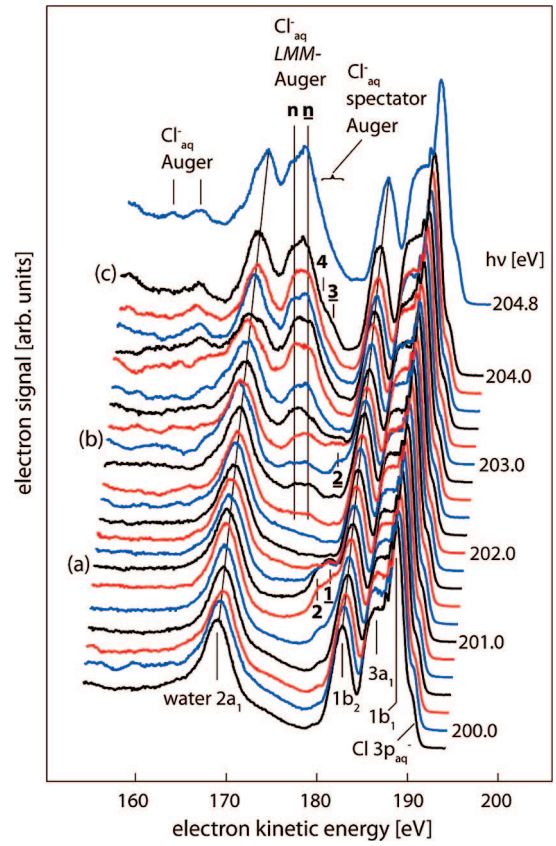

Figure 2. Photoelectron spectra from a 3 m LiCl aqueous solution measured for a series of photon energies near the Cl^-_{aq} 2p electron detachment energy. Intensities of the spectra were normalized to the $1b_1$ photoemission peak of liquid water. Normal Auger peaks associated with the Cl^-_{aq} $2p_{3/2}$ (n) and Cl^-_{aq} $2p_{1/2}$ (n) *LMM*-Auger process occur at constant kinetic energy, whereas constant-BE features move with the photon energy. Resonant absorption, corresponding to the promotion of a Cl^-_{aq} 2p electron into a series of empty CTTS-type states, gives rise to the readily visible spectator Auger electron peaks 2, 1, 2, 4, and 3. Here, the underline refers to excitation from Cl^-_{aq} $2p_{1/2}$; no bar refers to Cl^-_{aq} $2p_{3/2}$. Traces (a) and (b) depict the spectra for which the resonance features have maximum intensity.

valence holes (2 h). The corresponding spectral signature of 2h1e states should be a linear increase of KE as a function of photon energy, reflecting constant BE, similarly to one-hole (1 h) states.

When increasing the photon energy to $E_2 = 202.4$ eV (1.4 eV higher than E_1) a small peak **2** appears at a slightly higher

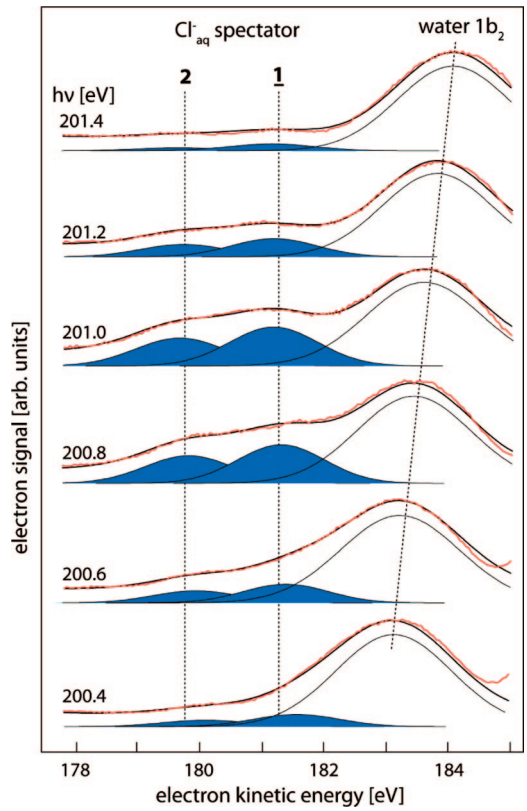

Figure 3. Zoom into the region of spectator Auger-electron peaks **2** and **1** (of Figure 2), showing the signal evolution as a function of photon energy. Blue peaks are Gaussian fits to **2** and **1**. The individual Gaussians to the water features are not shown here.

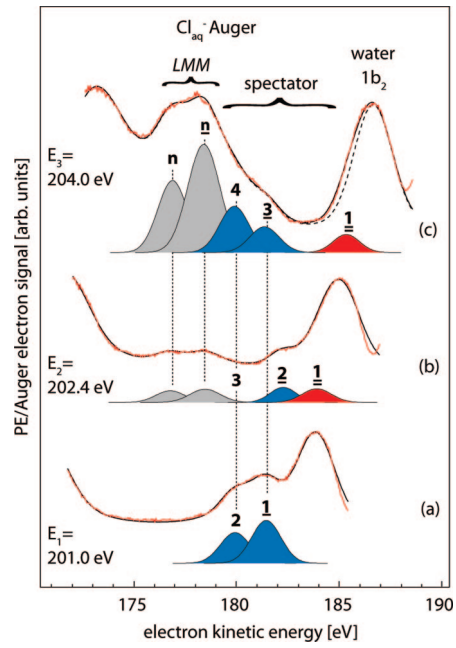

Figure 4. Zoom into the region of spectator Auger peaks of the spectra (a)−(c) of Figure 2, corresponding to E_1, E_2, E_3 absorption maximum, respectively. Gaussian fits are presented for the resonance peaks (red and blue) and for the normal Auger peaks (gray). Peak **1** results from a shakedown-like relaxation process or internal conversion to the fully relaxed lowest state. The dashed curve is the fit to the spectrum in the absence of peak **1**.

KE as compared to **1** (Figure 2, trace b). Peak **2** disappears at the next higher photon energy of 202.6 eV, but at a further photon-energy increase to $E_3 = 204.0$ eV (1.6 eV higher than E_2), the small shoulders **3** and **4** appear in the spectrum (Figure 2, trace c). As mentioned in the Introduction, we assign these three resonances, E_1, E_2, and E_3, of the aqueous chloride anion to excitations into the lowest and higher CTTS states, respectively. At a given energy E_i electrons from Cl $2p_{1/2}$ and Cl $2p_{3/2}$ can be promoted simultaneously, however, into different CTTS states. Interestingly, none of these resonances were observed at E_1, E_2, and E_3 in our separately conducted fluorescence yield measurements upon X-ray absorption, likely because the Auger electron yield is strongly favored over the *L*-shell fluorescence yield at this low atomic number.[37]

In order to better visualize and to accurately quantify the rather small spectral changes related to resonant and normal Auger-electron emission in the series of Figure 2, we now look in more detail at the spectral regions of interest. An enlarged detailed view of the spectra associated with the *first* resonance (near E_1) is presented in Figure 3, showing the evolution of peaks **2** and **1** as a function of excitation photon energy. Intensities of the spectra in Figure 2 were normalized with respect to the water $1b_2$ direct photoemission signal intensity. The blue-filled peaks are the respective single-Gaussian fits to **2** and **1**; the Gaussians fitted to the PE features were omitted for clarity. Peak widths of **2** and **1** are identical, 2 eV, and the intensity ratio **1**/**2** is nearly constant with a value of ∼1.5. If **2** and **1** were associated with nonresonant states, these peaks should show a linear KE increase as a function of photon energy, similarly to the solvent $1b_2$ band. In Figure 3, however, the resonance bands **2** and **1** exhibit a small red shift for the photon-energy increase from 200.4 to 201.4 eV. This kind of negative photon energy dependence was discussed previously.[38] If the spectator electron was in a completely localized state like a discrete state in the isolated atom system, the photon energy dependence would be −1.[39] On the other hand, if the spectator electron was in a completely delocalized state like a conduction band in the metallic system, no photon-energy dependence would be observed.[38] Hence, the present negative photon energy dependence of ∼ −0.5 indicates that the spectator electron is neither completely localized nor completely delocalized but is rather weakly localized around the chlorine atom in the aqueous solution, similarly to the case of ionic molecular crystals.[38] From Figure 3 the Cl^-_{aq} $2p_{3/2}$ (**2**) and Cl^-_{aq} $2p_{1/2}$ (**1**) absorption fwhm is determined to be ∼0.7 eV, which is difficult to determine in the absorption spectrum itself due to the very weak excitonic interaction.

Enlarged detailed views of spectra for the second (E_2) and third (E_3), and also for the first (E_1) resonance, presented in Figure 4, reveal the principal resonant Auger spectral features. The spectra of Figure 4 are the traces a, b, and c of Figure 2. The filled peaks are Gaussian fits with the same 2 eV fwhm as determined in Figure 3. Only Gaussians for the extra resonance peaks as well as for the normal Auger peaks are shown for clarity. It is important to note that in fitting the water $1b_2$ contribution a Gaussian with an identical width was used for all spectra in Figure 4. The spectrum at photon energy E_1 (Figure

(37) Stöhr, J. *NEXAFS Spectroscopy*; Springer Verlag: Berlin, 1992.

(38) Takata, Y.; Hatsui, T.; Kosugi, N. *J. Electron Spectrosc. Relat. Phenom.* **1999**, *103*, 443.

(39) Ueda, K.; West, J. B.; Kabachnik, N. M.; Sato, Y.; Ross, K. J.; Beyer, H. J.; Hamdy, H.; Kleinpoppen, H. *Phys. Rev. A* **1996**, *54*, 490.

4, trace a) exhibits the resonance peaks **2** and **1**, at 179.7 and 181.2 eV KE, as already seen in Figure 3. At photon energy E_2 (Figure 4, trace b) Cl^-_{aq} 2p normal Auger peaks **n** and **n**, at 177.0 and 178.5 eV KE, are observed with low intensities. Yet the peaks are well resolved in contrast to the spectrum measured far above the threshold (Figure 1), and the **n/n** intensity ratio of almost unity, instead of approximately 0.5 as for off-resonance excitation (see Figure 1), reflects the lower Cl^-_{aq} $2p_{3/2}$ ionization threshold energy as compared to Cl^-_{aq} $2p_{1/2}$. In addition to the normal Auger peaks three new peaks, **3**, **2**, and **1**, with 179.9, 182.3, and 183.9 eV KE, respectively, can be resolved in the E_2 spectrum of Figure 4. They are attributed to resonant excitation, similar to **2** and **1** at E_1. Then, at photon energy E_3 normal Auger peaks **n** and **n** increase in intensity, with the **n/n** intensity ratio considerably increasing as expected for above-threshold ionization. Furthermore, three additional peaks **4**, **3**, and **1** appear at E_3. Peaks **4** and **3** have KEs of 180.0 and 181.5 eV, which are almost the same as those for **2** and **1** at E_1, but the binding energies (BEs) of **4** and **3** at E_3 are almost 3.0 eV higher than those of **2** and **1** at E_1, as can be directly seen by the energy separations from the water 1 h ($1b_2$) state. For comparison we also present in spectrum (c) of Figure 4 the total spectral fit in the absence of peak **1** (dashed curve) to emphasize the importance of this spectral feature. The single peak **1** occurs at a KE of 185.5 eV and has the same binding energy, 18.5 eV (= 204.0 − 185.5), as that of peak **1** (KE of 183.9 eV, BE = 202.4 − 183.9) at E_2, but a different binding energy from peak **1** at E_1 (201.0($h\nu$) − 181.2(KE) = 19.8 eV(BE)). Energies of all resonance peaks observed here are summarized in Table 1, where TE (term energy) for each 2h1e final state is the difference between BE (2h1e) and DIP (2 h) (double Cl 3p ionization potential) relative to the ground state. DIP (2 h) = 25.1 eV is evaluated by using BE(Cl $2p_{3/2}$) = 202.1 eV and BE(Cl $2p_{1/2}$) = 203.6 eV, and the normal Auger KE($2p_{3/2}$) = 177.0 eV and KE($2p_{1/2}$) = 178.5 eV

Given the relatively small spectral changes associated with Cl^-_{aq} 2p resonant excitation, analogous measurements were performed for 2 M NaCl aqueous solution in order to evaluate the effect of the countercation on the spectra. Comparison of the spectra for the two chloride solutions (not shown), measured at identical photon energies, confirm the very same resonance behavior that was highlighted in Figure 4. These include the small peak **2**, which also for NaCl only shows up within the very narrow photon energy range 202.3−202.5 eV. Likewise, the evolution of the **4**-, **3**-shoulder is the same for the two solutions. As a side result, from the PE intensity ratios in Figure 4 we find that the absolute cross section Cl 2p to CTTS resonant absorption is on the order of 0.5×10^{-18} cm^{-2}.

Discussion

Origin and Evaluation of Spectral Resonance Features in a Simplified Energy-Level Diagram Model. For a first-step semiquantitative explanation of the resonant excitation processes observed in the photoinduced Auger-electron spectra of Figures 2–4, we consider the simplified energy-level diagram of Cl^-_{aq} shown in Figures 5 and 6. Normal Auger decay is illustrated in Figure 5a, while Figure 5b and c depict spectator Auger decay; Figure 5c in addition illustrates relaxation processes, so-called shakedowns. The various initial excitation transitions from Cl^-_{aq} $2p_{3/2}$ and Cl^-_{aq} $2p_{1/2}$ are explicitly assigned in Figure 6.

The normal *LMM*-Auger decay (Figure 5a), occurring for excitation photon energy exceeding the Cl^-_{aq} 2p binding energy, involves filling of a Cl^-_{aq} 2p hole (one-hole (1 h) state) by a

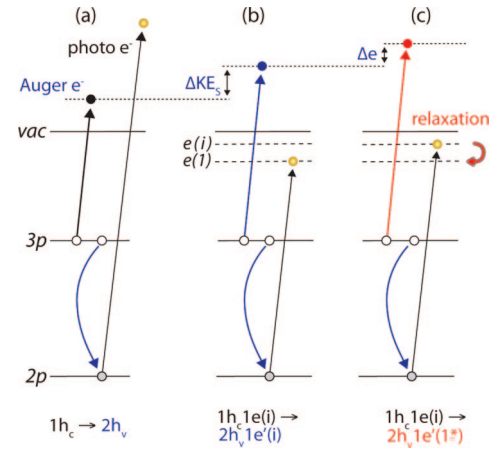

Figure 5. Schematic representation of Auger processes associated with 2p core-hole excitation of the chloride anion, Cl^-_{aq}, in aqueous solution. (a) Normal Auger decay, following the direct photoionization of Cl^-_{aq} 2p, results in 2 h final state. The kinetic energy of the normal Auger electron is 177.0 and 178.5 eV for Cl^-_{aq} $2p_{3/2}$ and Cl^-_{aq} $2p_{1/2}$ electron detachment, respectively. (b) Spectator Auger decay after 2p → e(1) resonant excitation, resulting in 2h1e final state. e(i) denotes a higher CTTS state. The Auger decay 1 h_c1e(i) → 2 h_v 1e′(i) is illustrated by blue arrows; the respective final state energies e′(i) are not shown. Subscripts c and v denote a core and valence hole, respectively. (c) Spectator Auger decay with shakedown processes (illustrated by the red arrow) 1 h_c1e(i) → 2 h_v1e′(1*), for i = 2 and 3. This results in a further increase of the Auger electron kinetic energy. Here e′(1*) indicates that the electronically relaxed state is lower in energy than e(1).

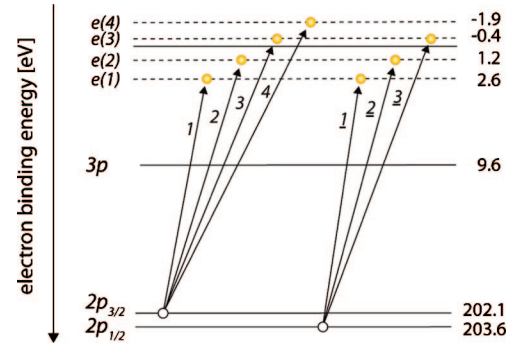

Figure 6. Schematic of X-ray absorption transitions from Cl^-_{aq} 2p into CTTS states. Resonance X-ray energies and binding energies for Cl^-_{aq} 3p and Cl^-_{aq} 2p given in the figure are from Figure 1 and from ref 35, respectively. Transitions **1**−**4** refer to electron promotion from Cl^-_{aq} $2p_{3/2}$, and **1**−**3** are the corresponding transitions from Cl^-_{aq} $2p_{1/2}$. The labels match with the labels in Figures 2−4. The resonance energies are 199.5 (**1**), 200.9 (**2**), 202.5 (**3**), 204.0 (**4**), 201.0 (**1**), 202.4 (**2**), and 204.0 (**3**) eV. These values correspond directly to the photon energy at which a given resonance exhibits a maximum spectator Auger-electron signal (compare Figures 3 and 4). Note that transitions **2** and **1** and transitions **3** and **2** have almost the same energies, respectively. Energy values of e(i), shown at the right-hand side, are the difference between the Cl^-_{aq} 2p binding energy and the respective E_i absorption maximum.

Cl^-_{aq} 3p electron and the subsequent release of an Auger electron at the characteristic "normal" KE, resulting in a two-hole (2 h) final state. This is a two-step process, and the normal Auger electron produced from the second step (1 h → 2 h) has a constant kinetic energy if we neglect some threshold effects such as postcollision interaction between the photoelectron and Auger electron. The spin−orbit splitting of the Cl^-_{aq} 2p level gives rise to two KE components (**n** and **n**) in the spectra.

Resonant X-ray absorption prepares the initial 1h1e (one-hole one-electron) state (Figure 5b and c), which leads to a situation where the Auger electron is released in the presence

of an extra excitonic electron (1e′), the so-called spectator electron (1e = 1e′). This final state is not a 2 h but rather a 2h1e′ (two-hole one-electron) configuration. The presence of the excited spectator electron (1e′) causes an increase in KE (denoted KE_s in Figure 5b) of the emitted Auger electron due to Coulomb interaction with 1e′ and a nonconstant KE for the photon energy as seen in Figure 4. Normal and spectator Auger-electrons can hence be directly distinguished by their KE in the aqueous-solution spectra, [40] and the occurrence of spectator Auger electrons is a signature of the empty states, and in certain cases even of the relaxation dynamics (see Figure 5c). An interesting situation arises if the excited electron delocalizes into the solvent within the time scale of Auger decay, in which case the same 2 h final state as that for normal Auger decay is reached. If the CTTS electron can couple to the conduction band of the solvent, this electron is no more bound by $Cl(2p)^{-1}$ or $Cl(3p)^{-2}$, and the normal Auger peaks observed at E_2 (Figure 4b) may be related to this channel. Yet another process relevant for the present work is electronic relaxation (shake down) from CTTS higher states into the CTTS lowest state, as depicted in Figure 5c. Here, an additional Auger peak arises, at a higher kinetic energy than that in the spectator Auger case without electronic relaxation from e(i) to e(1).

Figure 6 assigns the excitations from Cl^-_{aq} $2p_{3/2}$ and Cl^-_{aq} $2p_{1/2}$ into CTTS states observed in the experiment (Figure 4). Cl^-_{aq} binding energies shown in the figures were obtained from Figure 1 (202.1/203.6 eV for Cl^-_{aq} 2p) and from our previous work (9.6 eV for Cl^-_{aq} 3p).[35] Note, however, that the ionization energy of aqueous Cl^-_{aq} 2p has not necessarily a unique value, but a band of values, similar to the heterogeneous broadening found earlier for the O1s ionization energy for liquid water.[41]

Likewise, the observed (E_1) absorption width for the CTTS, 0.7 eV fwhm, largely results from the statistical distribution of solvation-shell configurations, leading to slightly different stabilization energies and, hence, to a (narrow) range of different CTTS transition energies. This is consistent with a small red shift of the CTTS states for the photon energy increase as already discussed in Figure 3.

Arrows in Figure 6 with the origin at Cl^-_{aq} 2p represent the X-ray absorption transitions into CTTS states, leading to the 1h1e state (see Figures 5b and 5c). Transitions, **1**−**4**, corresponding to electron promotion from the Cl^-_{aq} $2p_{3/2}$ level into CTTS states e(1), e(2), e(3), and e(4) are depicted at the left-hand side of the figure. The analogous transitions from Cl^-_{aq} $2p_{1/2}$, **1**−**3**, are shown at the right-hand side. We can then determine absolute CTTS energies as the difference between the Cl^-_{aq} 2p BE and the resonance energies E_i. The procedure is analogous to determining the empty state energies of liquid water, where final state energy differences from core vs valence hole were found to be small.[40] With E_1 (201.0 eV), corresponding to the electron promotion Cl^-_{aq} $2p_{1/2} \rightarrow$ 1h1e(1) (transition **1**) and Cl^-_{aq} $2p_{3/2} \rightarrow$ 1h1e(2) (transition **2**), the term energies (TEs) are TE = 2.6 eV for 2h1e′(1) and TE = 1.1−1.2 eV for 2h1e′(2). Here we have assumed that the detachment thresholds of the CTTS electrons are the same as those of the Cl 2p detachment thresholds, 203.6 eV for Cl^-_{aq} $2p_{1/2}$ and 202.1 eV for Cl^-_{aq} $2p_{3/2}$, where TE is a relative energy to the detachment thresholds of the CTTS electron. This places e(1), i.e., the CTTS lowest state, at 2.6 eV (see Figure 6) and can be used to find the energy of transition **1**, Cl^-_{aq} $2p_{3/2} \rightarrow$ 1h1e(1), which is 199.5 eV. The reason transition **1** is not observable at 199.5 eV photon energy in Figure 2 is that the corresponding spectral signature overlaps with the Cl^-_{aq} 3s photoemission peak. Similarly, we can determine the higher e(i) energies, or the respective TEs. From **2** and **3** at the second resonance E_2 (202.4 eV), we find TE = 1.2 eV for 2h1e′(2) and TE = −0.4 eV for 2h1e′(3), and from **3** and **4** at the third resonance E_3 (204.0 eV), TE = −0.4 eV for 2h1e′(3) and TE = −1.9 eV for 2h1e′(4). Here, a negative TE would imply a continuum state or antibonding resonance state, under the assumption of a unique threshold energy 202.1 eV for the Cl^-_{aq} $2p_{3/2}$ electron and 203.6 eV for the Cl^-_{aq} $2p_{1/2}$ electron. However, the Cl 2p electron binding energy has some distributions, dependent on short-range and long-range solvent coordination to Cl^-, which may result in a delayed ionization onset due to threshold effects such as postcollision interaction. Therefore, e′(4) may in fact not be a continuum state. If 2h1e′(i), i = 1−4, were all bound states, we have to assume the detachment threshold of the CTTS electrons of 1h1e(i) is above 204.0 eV. If the detachment threshold of the CTTS electron and the detachment threshold of Cl^-_{aq} 2p coincide, we cannot explain the coexistence of normal Auger and CTTS electrons at E_2 and E_3 in Figure 4, unless it is an antibonding resonance state.

The CTTS energies 1h1e(1) of TE = 2.6 eV and 1h1e(2) of TE = 1.1−1.2 eV (Figure 6) are in good agreement with previous experimental data from optical absorption. The measured ultraviolet CTTS-band maximum of chloride in water at 2 °C (the temperature in the present study is 4 °C) is 7.13 eV.[42] With 9.6 eV[35] BE for Cl^-_{aq} 3p, this yields TE = 2.47 eV for the CTTS energy, which compares very favorably with TE = 2.6 eV derived here. Transient optical absorption from the lowest CTTS state exhibits a maximum at 1.1 μm (1.13 eV),[9] which can be assigned to excitation into the second CTTS state (namely, the first excited CTTS above the lowest CTTS), provided the symmetry nature of the level allows for the optical dipole excitation. The higher CTTS states, corresponding to 1h1e(3) and 1h1e(4), have not been reported before. The present experiment is indeed unique, not only due to its one-photon excitation capabilities but also considering that the dipole excitation to 1h1e states is definitely a transition from Cl 2p core (1 h) to s-type (1e) levels, and the excited electron 1e′ is strongly bound by 2 h states with $3p^{-2}$ configurations after the spectator Auger decay.

Probably the most interesting feature in Figure 4 is peak **1** observed at E_2 and E_3, which are the resonance energies for the second to fourth CTTS states, e(i), i = 2−4, but are not the resonance energy for the lowest CTTS state e(1). Hence the experiments clearly indicate that the spectator electron in e′(i), i = 2−4, is effectively relaxed (shaken down) to the lowest CTTS state e′(1*), where * means that the spectator electron is not in a rigid state but rather in a relaxed state. This process has been depicted in Figure 5c. Our interpretation is indeed corroborated by Table 1, showing that the lowest CTTS state e′(1) has TE = 5.3 eV at the e(1) resonance energy E_1, but the lowest CTTS state e′(1*) has TE = 6.6 eV at E_2 and E_3. This implies that the 1h1e CTTS states e(2)−e(4) have internally converted to e′(1*) but not directly to e′(1) itself. The internal conversion from e′(1) to e′(1*) is found to be associated with 1.3 eV of relaxation energy. This is the first report for direct

(40) Winter, B.; Hergenhahn, U.; Faubel, M.; Björneholm, O.; Hertel, I. V. *J. Chem. Phys.* **2007**, *127*, 094501.
(41) Winter, B.; Aziz, E. A.; Hergenhahn, U.; Faubel, M.; Hertel, I. V. *J. Chem. Phys.* **2007**, *126*, 124504.
(42) Fox, M. F.; Barker, B. E.; Hayon, E. *J. Chem. Soc., Faraday Trans. 1* **1978**, *74*, 1776.

evidence of internal conversion in the ultrafast electron dynamics of higher CTTS excited states.

Comparison with ab Initio Calculations. We have calculated, for four different cluster models of ~2 M NaCl and LiCl aqueous solutions, term energies of 1h1e(i) and 2h1e′(i) relative to the 1 h and 2 h states, average size of e(i) and e′(i) orbitals, binding energies (BE) of the Cl 2p core-ionized state (1 h), and the double ionization potential (DIP) of the lowest Cl $(3p)^4$ triplet final state, for four different cluster models of ~2 M NaCl and LiCl aqueous solutions. 2h1e′(i) is calculated by keeping e′(1) the same as e(i) as in 1h1e(i). 2h1e′(1*) is a fully relaxed state, and 2h1e′(1) is an unrelaxed state. These results are summarized in Table 2, in comparison with the experiments for 1h1e (Cl 2p) CTTS and 2h1e′ (spectator Auger decay) CTTS. The Cl 2p ionization potential (BE) 204.2−204.3 eV overestimates the experimental values, 202.1 and 203.6 eV. This disagreement may be due to incomplete electrostatic stabilization within the present four model calculations. Here, the Cl 2p CTTS states 1h1e(i), $i = 1-4$, are all bound states; that is, TEs in the 1h1e states are all positive, in disagreement with the experimental values, which are evaluated by neglecting a delayed onset due to threshold effects. The lowest theoretical TE 2.5−2.8 eV is in good agreement with the experiment 2.6 eV, but theoretical TEs disagree with the experiment for the higher states.

Table 2 shows double ionization potentials (DIPs) of Cl $3p^{-2}$ 2 h states. The calculated DIP 26.5−27.0 eV overestimates the experimental value 25.1 eV. Similarly to the case of Cl 2p BE, this disagreement may be due to incomplete electrostatic stabilization within our model calculations. Tables 1 and 2 show experimentally and theoretically the CTTS states with double valence hole states 2h1e′ all being bound states below DIP. The situation is obviously different from the CTTS states with Cl 2p hole states 1h1e. As shown in Tables 1 and 2, the experimental TE of the lowest 2h1e′(1) state is 5.3 eV at E_1, but the TE of the 2h1e′(1*) state is 6.6 eV at E_2 and E_3. This means 2h1e′(1*) is not the same state as 2h1e′(1). The calculated TE of 2h1e′(1) using the same e(1) orbital as that in 1h1e(1) is 4.6−6.0 eV, and the TE of the fully relaxed lowest 2h1'e(1*) state is 6.8−7.2 eV. The result is in agreement with the experiment, indicating that in the CTTS states without electronic relaxation the spectator electron e(1) is almost unrelaxed (frozen) during the spectator Auger decay to e′(1). The higher CTTS states also show reasonable agreement in term energy between theory and experiment. On the other hand, after the spectator Auger decay with shakedown, the spectator electron e(1) is fully relaxed to e′(1*), where * refers to self-consistent results and e′(i) corresponds to frozen results from e(i) with keeping the orbital size. We also notice that the orbital size of e′(1*) (4.0−4.8 Å) becomes more compact than e′(1) = e(1) (6.0−6.7Å) after relaxation under double valence holes. The present observation of relatively strong relaxation features indicates the importance of electron dynamics in CTTS states during the spectator Auger decay.

Another interesting observation is that the experimental assignment, in Table 1, for 2h1e′(2) shows TE = 3.8 eV (Cl $2p_{3/2}$) at E_1 and TE = 5.0 eV (Cl $2p_{1/2}$) at E_2. The latter may correspond to TE = 5.3 eV for 2h1e′(1). Thus, the assignment of peak **2** at E_2 in Figure 2 remains yet to be resolved, considering that the resonance width is very narrow, from 202.3 to 202.5 eV. We may have to associate peak **2** with e′(2*), where the energy difference in TE between e′(2) and e′(2*) is 1.2 eV and can be due to electronic relaxation as already discussed for e′(1*).

Previously, a series of bound CTTS states was also reported using quantum molecular dynamics simulations of Cl^- in water.[11,13] The computed density of states of an *s*-like CTTS lowest state (termed 4*s*) was found to have a maximum at −2.5 eV, well in agreement with values reported here. Near −1.4 eV, the calculations revealed a dense manifold of states, followed by a region of *p* symmetry and then one of *s*/*d* symmetry, joining into the continuum.[11,13] Notice that the state of *p* symmetry is forbidden for dipole transitions from the Cl 2p. Moreover, the computed transient CTTS absorption spectrum, right after the photoexcitation, peaks at 1.1 eV, which corresponds to one-photon transitions between the 4s and higher *p*-like CTTS states of aqueous chloride.

Quantum nonadiabatic molecular dynamics simulations of the relaxation dynamics, following two-photon (UV) excitation of an aqueous halide ion, have addressed detachment of a CTTS electron as a pathway of producing a solvated electron.[12] Two channels that branch within less than 50 fs were observed, and it is these processes that may be relevant to the current experiment despite the different preparation scheme. The dominant channel is similar to the relaxation observed here; i.e., the electron relaxes into lower energy states of the CTTS manifold within this very short time. The minor channel of the simulation corresponds to direct detachment, involving relaxation of the initially excited ion via a nonadiabatic transition into the solvent conduction band. Detachment through either channel eventually results in a final state of a halogen atom and solvated electron. Our experiment probes both these channels, as higher CTTS states that decay in <10 fs via nonadiabatic coupling into the delocalized solvent conduction band should give rise to a signal in the region of the normal Auger peaks, whereas states that decay by internal conversion into lower CTTS states give rise to the additional spectator Auger peaks observed. Further analysis may allow this branching to be quantified. Notice that direct electron detachment on a time scale *longer* than the Auger decay is unlikely for the lower 2h1e states with larger TEs than 2.5 eV, where a CTTS electron is strongly bound by Cl $3p^{-2}$. However, 1e(3) in 2h1e has a TE = 2.6 eV and is similarly bound to the 1e(1) in 1h1e (Cl valence and core); therefore, the higher 2h1e CTTS states might behave similar to Cl valence CTTS states, with the possibility of electron detachment and formation of a solvated electron.

Conclusions

Charge-transfer-to-solvent (CTTS) excited states of aqueous chloride are studied by resonant inner-shell photoexcitation, Cl^-_{aq} 2p → e(i), $i = 1-4$, which denotes a series of excitations to CTTS lowest and higher states. The CTTS excitation from the Cl 2p level is invisible in conventional (X-ray) photoabsorption experiments. We have successfully detected the CTTS states by measuring the resonance Auger electrons emitted following the Cl 2p excitation to the CTTS state. The excitation cross sections for the resonant processes are on the order of 0.5 Mb. During the resonance Auger decay the CTTS electron behaves like a spectator, which can be easily distinguished in the present experiment due to the inherent two-dimensional nature of the recorded spectra (photon energy and electron kinetic energy). In the Auger final state the CTTS electron is strongly bound by two valence

hole states. The small negative photon-energy dependence of the lowest spectator Auger decays indicates the weakly localized character of the CTTS electron as shown in Figure 3. Furthermore, in Figure 4, we found for the first time that the CTTS electron e(i) bound by a single Cl 2p hole shows relaxation dynamics to the lowest state, e′(i) → e′(1*), bound by a double Cl 3p-valence hole state after the spectator Auger decay. The present interpretation is supported by ab initio calculations. Liquid-jet studies as performed here not only demonstrate the strength of liquid photoelectron spectroscopy to complement ultrafast laser-pump−probe absorption studies but also highlight particularly the potential of using resonance core-level excitations to explicitly characterize early time relaxation dynamics in aqueous solutions. The characterization of the CTTS excited states dynamics is an important step forward toward a better understanding of how the solvent responds to the ultrafast movement of charge, which is at the heart of many photon induced processes in aqueous chemistry and biology.

Acknowledgment. We thank Stephen E. Bradforth and Christopher G. Elles for many stimulating discussions and the BESSY staff, especially Gerd Reichardt and Rolf Follath, for support at the beamline. B.W. gratefully acknowledges support by the Deutsche Forschungsgemeinschaft (Project WI 1327/3-1).

Supporting Information Available: Cartesian coordinates of the optimized structures and the complete ref 20. This material is available free of charge via the Internet at http://pubs.acs.org.

JA8009742